PHYSICAL REVIEW B **84**, 064404 (2011)

Evidence of defect-induced ferromagnetism in $ZnFe_2O_4$ thin films

C. E. Rodríguez Torres,[1] F. Golmar,[2,*] M. Ziese,[3] P. Esquinazi,[3] and S. P. Heluani[4]
[1]*IFLP-CONICET and Departamento de Física, Facultad de Ciencias Exactas, Universidad Nacional de La Plata, C.C. 67 (1900) La Plata, Argentina*
[2]*CIC nanoGUNE Consolider, Tolosa Hiribidea 76, 20018 Donostia, Spain*
[3]*Division of Superconductivity and Magnetism, University of Leipzig, D-04103 Leipzig, Germany*
[4]*Laboratorio de Física del Sólido, Dpto. de Física, FCEyT, Universidad Nacional de Tucumán, Tucumán, Argentina*

(Received 21 January 2011; revised manuscript received 14 April 2011; published 11 August 2011)

X-ray absorption near-edge and grazing incidence x-ray fluorescence spectroscopy are employed to investigate the electronic structure of $ZnFe_2O_4$ thin films. The spectroscopy techniques are used to determine the nonequilibrium cation site occupancy as a function of depth and oxygen pressure during deposition and its effects on the magnetic properties. It is found that low deposition pressures below 10^{-3} mbar cause iron superoccupation of tetrahedral sites without Zn^{2+} inversion, resulting in an ordered magnetic phase with high room-temperature magnetic moment.

DOI: 10.1103/PhysRevB.84.064404 PACS number(s): 61.05.cj, 75.25.−j, 75.30.−m, 75.50.Bb

I. INTRODUCTION

Among the functional materials that are being studied intensively to fabricate novel spintronics devices, the spinel oxides appear as an important alternative to perovskites. In particular, $ZnFe_2O_4$ can be a half-metallic, transparent conductor or ferrimagnetic insulator.[1,2] At low dimensions, changing the growth conditions, the magnetic and electronic properties of the ferrites can be tuned to enhance the magnetic moment considerably and to produce conducting or insulating materials.[3] These properties are very important for the design and fabrication of multilayer structures to produce spin-polarized currents.

It is well known that bulk $ZnFe_2O_4$ crystallizes in the normal spinel lattice and that it is antiferromagnetic with a Néel temperature of about 10 K. Zn^{2+} occupies tetrahedral (A) and Fe^{3+} octahedral (B) sites. The interaction between magnetic Fe^{3+} moments is of superexchange type mediated by O^{2-} ions and results in the magnetic moments being antiparallel to each other. Since the superexchange interaction is stronger for the more closely situated cations and for the bond angle closer to 180°, the superexchange interaction of A-O-B (J_{AB}) is the strongest, the B-O-B (J_{BB}) is weaker, and that of A-O-A (J_{AA}) is the weakest. Accordingly, the magnetic structure and properties of spinel-type oxides depend strongly on the relative strength of the various superexchange interactions. In a normal spinel, magnetic Fe^{3+} ions occupy only B sites and the weak negative superexchange interaction among Fe^{3+} ions (J_{BB}) dominates the magnetic properties of $ZnFe_2O_4$ leading to a low Néel temperature and, consequently, paramagnetic behavior at room temperature. The situation is different, however, when normal spinel ferrite becomes nanosized. Net magnetization at room temperature can be obtained for nanoparticles obtained by different methods, such as mechanical synthesis,[4–6] solvothermal method,[7] sol-gel,[6] co-precipitation,[3,8] and thin films deposited by sputtering[9] and by pulsed laser deposition.[10] Several works have suggested that, in this case, the ferrite displays a nonequilibrium cation distribution among the tetrahedral and octahedral sites altering its long-range magnetic ordering. As a consequence, the magnetic response is drastically enhanced. It was reported that when the particle size decreases, Fe^{3+} occupancy of both A and B sites in the nanocrystalline state changes and Zn ions are transferred from their equilibrium position sites A to B sites. However, there is still some lack of clarity concerning Zn nonequilibrium positions and their magnetic effects. It is thought that the occupation of B sites by Zn^{2+} brings Fe^{3+} ions in both A and B sites, and the strong superexchange interaction between Fe^{3+} ions in A and B sites forces Fe in B sites to align ferromagnetically, causing high magnetization at room temperature.[5,6,8,11,12] In addition, several authors reported the clear dependence of magnetic response on the preparation process, apart from the particle size.[13,14] Furthermore, it was found that both the magnetic properties and cation distribution are extremely dependent on deposition conditions.[10,15]

Despite progress in the characterization, the spin configuration of nanosized ferrites is still unclear and under study.[16] As the spinel oxides are ferrimagnets involving two different sublattices, the resulting magnetic moment is strongly perturbed by defects in the structural lattice. In addition, there has been increasing evidence that magnetic order can be triggered by certain defects in materials that are nominally nonmagnetic like certain oxides[17–19] or pure graphite.[20] In a thin-film deposition process, many of these defects can be generated. In particular, it was recently suggested that oxygen vacancies affect the magnetic properties of synthesized Zn-ferrite films grown at various oxygen pressures.[21] Also, the oxygen vacancies could be responsible for the semiconducting behavior found in $ZnFe_2O_4$ thin films with high saturation magnetization at room temperature and high Curie temperature.[10] There is clearly some need to employ new experimental procedures using different techniques that can provide complementary information that may clarify several open issues on the subject.[22]

The x-ray absorption near-edge structure (XANES) technique together with simulations based on *ab initio* XANES calculations such as code FEFF8.2 are powerful tools to identify the modification of Zn^{2+} and Fe^{3+} distribution from the equilibrium to the nonequilibrium state.[5,9,23,24] Additionally, grazing-incidence x-ray fluorescence (GIXRF) yields the composition, thickness, and density of thin films.[25,26]

XANES combined with GIXRF results in an interesting method to relate thickness-dependent electronic structure with magnetic properties.[27] XANES is not a surface technique by itself, since the attenuation length of hard x rays is a few micrometers in any material. However, in the grazing-incidence geometry near the critical angle for total reflection, the x-ray beam is confined within a few nanometers of the surface. For film studies, this confinement has the considerable advantage of minimizing the substrate contribution.

In this work, the structural and magnetic properties of $ZnFe_2O_4$ films fabricated by pulsed laser deposition using different oxygen partial pressures are reported and discussed. XANES spectroscopy combined with GIXRF was used to determine the nonequilibrium cation site occupancy as a function of depth and its effects on the magnetic properties. Our results show that the presence of defects as oxygen vacancies or iron situated on normally nonoccupied A sites in the spinel structure could be the cause for the magnetism in the films.

II. EXPERIMENTAL

The $ZnFe_2O_4$ films were fabricated by pulsed laser deposition (PLD) from a stoichiometric target onto MgO (001) substrates. Substrate temperature was 500 °C and the oxygen partial pressure varied between 10^{-5} and 10^{-1} mbar. After deposition, the samples were cooled to room temperature in vacuum at a pressure of about 10^{-7} mbar.

X-ray diffraction measurements employing Cu $K\alpha$ radiation in a Phillips X-Pert were made for a structural characterization diffractometer. Scanning electron microscopy (SEM), Supra 55VP, with energy-dispersive spectroscopy (EDS) was employed to study the surface morphology and spectral analysis. Magnetization measurements were made in a Quantum Design model MPMS-7 SQUID magnetometer. Magnetic fields were applied parallel to the films.

Electrical resistance measurements were performed using a Keithley 2182A Nanovoltmeter and a Keithley 6221 current source. Electrical contacts were made with gold wires clenched with indium. We have measured the resistance with a two-probe techniques.

GIXRF measurements were carried out at the XRF Fluorescence beamline of the LNLS (Campinas, Brazil), using a monochromatic x-ray beam of 9.7 keV. The setup includes 150-μm-vertical and 4-mm slits limiting the beam size on the sample mounted on a high-precision goniometer. Angular scans around the critical angle of total (external) reflection were performed (between 0° and 2°). The fluorescence emissions were collected using a 15-element Ge detector. After the angular scan, XANES Fe K edge (7112 eV) and Zn K edge (9659 eV) spectra in fluorescence mode were collected at different grazing angles using a Si (111) channel-cut monochromator. The incident beam intensity and the energy calibration were monitored using an ion-chamber and a Co (or Zn) metal standard. The reflected beam and the Co (or Zn) fluorescence emission were collected using a second ion chamber and a 15-element Ge detector, respectively.

Room-temperature extended x-ray-absorption fine-structure (EXAFS) spectra at the Zn K edge were recorded in fluorescence mode using a Si(111) monochromator at the XAS2 beamline of the LNLS (Laboratorio Nacional de Luz Sincrotron) in Campinas, Brazil. In order to estimate the x-ray penetration depth for each incidence angle, the attenuation length as a function of incidence angle was estimated using the x-ray database of Lawrence Berkeley National Laboratory.[28]

III. RESULTS AND DISCUSSION

X-ray diffractometry indicated epitaxial growth without any traces of secondary phases. φ scans of the $ZnFe_2O_4$ (511) refection showed a fourfold symmetry of the film. Figure 1 shows the magnetic moment of the films as a function of applied field at room temperature (a) and at 5 K (b). The diamagnetic signal from the substrate was subtracted. The S-shaped M-H curves are evidence for ferrimagnetic order. In addition, a linear high-field response in room-temperature measurements indicated the presence of a paramagnetic component. This was also deduced from M versus T measurements (not shown here). The magnetic response diminishes by increasing the oxygen partial pressure from 10^{-5} to 10^{-1} mbar as seen by the decreasing of the magnetic moment by more than one order of magnitude. While at room temperature the coercivity is small, at low temperatures the films are magnetically rather hard with coercive fields between 447 and 1000 mT when deposition pressure varied from $P = 10^{-5}$ to 10^{-1} mbar. The drastic reduction of coercive field at room temperature might indicate the existence of magnetic clusters and a blocking mechanism such as has been observed in Refs. 6 and 9 for similar systems.

All films are insulating with room-temperature resistivity larger than $\rho = 100\ \Omega$ m. Sample ZF02 grown under 10^{-4} O_2 pressure had the smallest electrical resistance and we could measure its behavior under applied magnetic fields between 0.2 and 0.7 T and under light irradiation between 2.8 and 3.5 eV. The sample presented neither magnetoresistance nor photoconductivity in the range of fields and energies applied. SEM micrographs show uniform surfaces in all samples. These results suggest that the sample has a spatial uniform magnetic phase at room temperature and that the energy gap in this sample is larger than 3.5 eV.

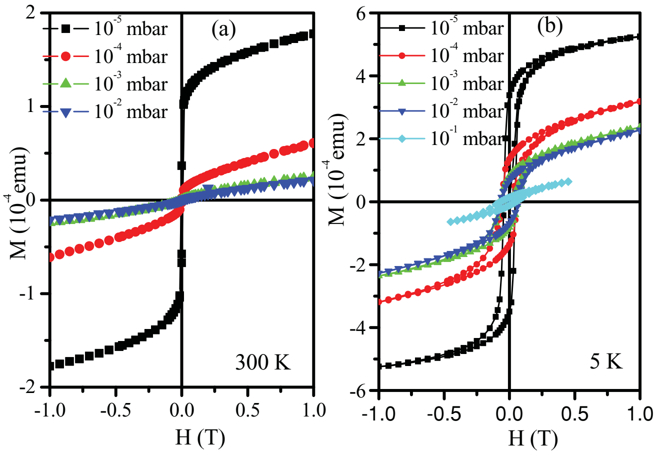

FIG. 1. (Color online) Magnetic moment as a function of applied field at room temperature (a) and at 5 K (b) for the films prepared at different partial pressures.

TABLE I. Measurement parameters of ZFO: Oxygen partial pressure p, film thickness t, Fe/Zn ratio, and magnetic saturation moment measured at room temperature and 5 K.

Sample	p (mbar)	t (nm)	Fe/Zn	M(RT) (10^{-4} emu)	M(5 K) (10^{-4} emu)
ZFO1	10^{-5}	57	1.8	1.4	5.0
ZFO2	10^{-4}	51	2.3	0.2	2.5
ZFO3	10^{-3}	43	1.9	0.1	1.9
ZFO4	10^{-2}	36			1.5
ZFO5	10^{-1}	17	1.8		0.3

In Table I, we summarized the results on the characterization of samples labeled as ZFO1 to ZFO5.

Using the thicknesses in Table I and the magnetic measurements, the estimated magnetizations for sample ZFO1 are 100 and 360 emu/cm^3 at room temperature and 5 K, respectively. These are large values considering that $ZnFe_2O_4$ with normal spinel structure is an antiferromagnet.

Figure 2 shows the intensity of Fe and Zn $K\alpha$ lines as a function of incident angle for all films. The intensities are in arbitrary units and there is no direct relationship between intensities and concentration. The angle where a jump in intensity was observed (approximately 0.32°) corresponds to the total reflection condition. It can be observed that Zn/Fe fraction remains constant for all angles, indicating a uniform distribution of both cations in depth. Furthermore, a Zn enrichment with the increase of oxygen pressure can be seen: the curve corresponding to Zn almost coincides with the Fe one for 10^{-5} mbar, and this is above the Fe one for $P = 10^{-1}$ mbar. The XRF results were confirmed by EDS (see Table I), although it can be seen that the ratio Fe to Zn is close to 2:1 independent of the O_2 growth conditions.

Figure 3 exhibits Zn (right) and Fe (left) K-edge XANES spectra, corresponding to samples 1, 2, and 5 taken at an incidence angle above total reflection (0.38°). The attenuation length for this angle was estimated as 35 nm, and then these spectra contain information from the inner part of the film. The spectrum of powder $ZnFe_2O_4$ normal spinel was included for comparison. Zn K-edge spectra of normal spinel have three resolved peaks, A, B, and C (indicated in Fig. 1), at around 9664, 9668, and 9672 eV, respectively, a shoulder at around 9677 eV (peak D), plus additional structure at higher energies (peak E). Zn K-edge spectra of samples 1 and 2 have similar characteristics to a normal spinel. This indicates that in these films, Zn ions are mostly on A sites. In the case of sample ZFO5, the increase of peak B indicates that there is an important fraction of Zn on B sites.[5,15,23]

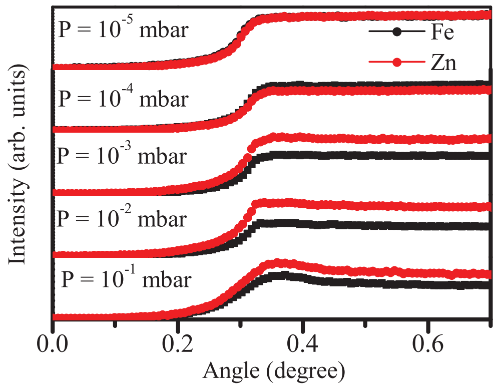

FIG. 2. (Color online) Intensity of Fe and Zn $K\alpha$ lines as a function of incident angle for all films. The intensities are in arbitrary units.

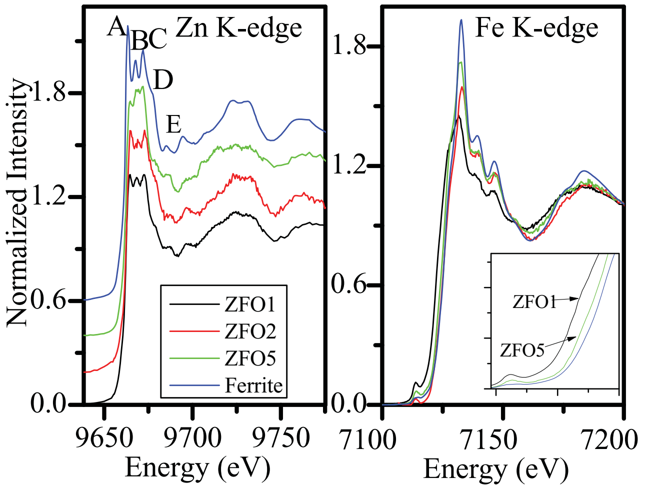

FIG. 3. (Color online) (a) Zn and (b) Fe K-edge XANES using an incident angle of 0.38° for films deposited at different oxygen pressures.

Concerning the Fe K edge, in the case of normal ferrite, the edge position is expected for an Fe^{3+} oxidation state and the pre-edge structure is characteristic of Fe in a distorted octahedrally coordinated environment that arises from electronic $1s \rightarrow 3d$ quadrupole and $1s \rightarrow 3d/4p$ hybridized orbital dipole transitions. In XANES spectra of samples 2 and 5, the edge positions are close to the $ZnFe_2O_4$ position but the white line amplitude is smaller, which could indicate the presence of Fe^{3+} with a coordination lower than 6.[5,15] Also the prepeak amplitude is higher than that corresponding to normal ferrite, indicating an increase of the degree of orbital p-d mixing that could indicate that the central Fe atoms occupy a more noncentrosymmetric environment.

The decrease of the white line and the increase of the prepeak intensities are larger for samples ZFO1 and ZFO2. Also, the shift of the edge to lower energies observed for ZFO1 indicates the presence of Fe^{2+}. This sample, which has the highest magnetic moment, has the lowest white line intensity, the highest prepeak amplitude, and the lowest-energy edge.

The increase of B peak on the Zn K-edge spectrum of ZFO5 could be indicative of inversion in a normal spinel, i.e., Zn^{2+} in B sites and Fe^{3+} in A sites. However, in the Fe K-edge spectrum, the changes, compared with a normal spinel, are minor and this film has the lowest Curie temperature and magnetic moment. In the case of ZFO2 and ZFO5, which are ferromagnetic at room temperature, according to the Zn K-edge spectrum, Zn ions are only in tetragonal A sites. Therefore, there is no inversion, but the decrease of the white line and the increase of the prepeak indicate a decrease of Fe oxygen coordination and probably an increase of Fe in the tetrahedral site.

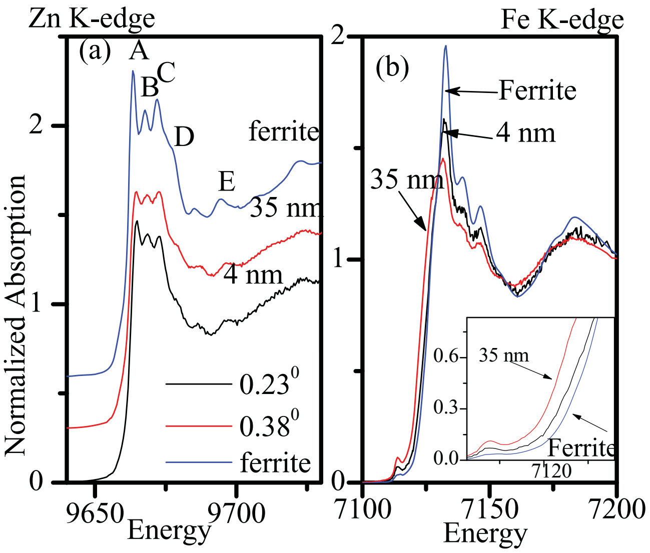

FIG. 4. (Color online) (a) Zn and (b) Fe K edge XANES, taken for film deposited at 10^{-4} mbar for two different incidence angles.

In order to study the differences between bulk and surface, we present now a comparison between XANES taken with incidence angle below and above the total reflection angle (0.23°, attenuation length around 4 nm, and 0.38°, attenuation length around 35 nm, respectively).

In the case of ZFO1 (Fig. 3), no major changes were observed in the Zn K edge. The decrease of peak C could be related to the elimination of multiple scattering paths due to the high contribution of surface atoms. The same can be observed for ZFO2 (see Fig. 4). In the Fe K edge, the changes that evidence an increase of Fe in A sites and/or vacancies in the B site octahedron are less pronounced at the surface. In the case of ZFO5 (see Fig. 5), the tendency is similar but the difference with the normal spinel is smaller.

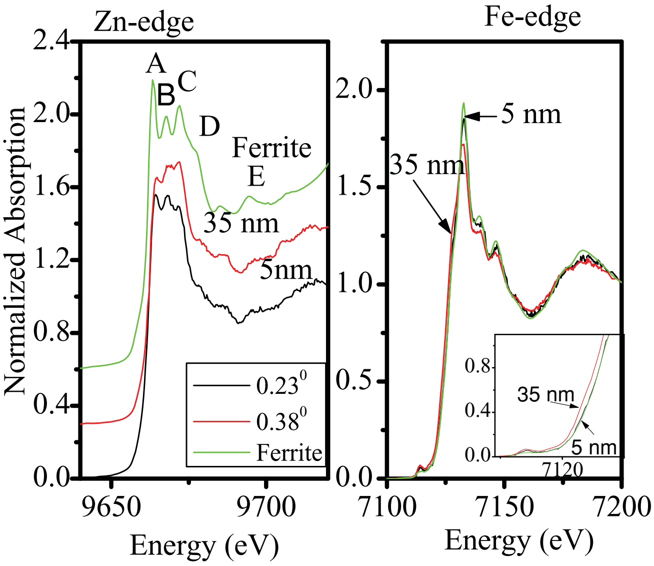

FIG. 5. (Color online) (a) Zn and (b) Fe K-edge XANES, taken for film deposited at 10^{-1} mbar for two different incidence angles.

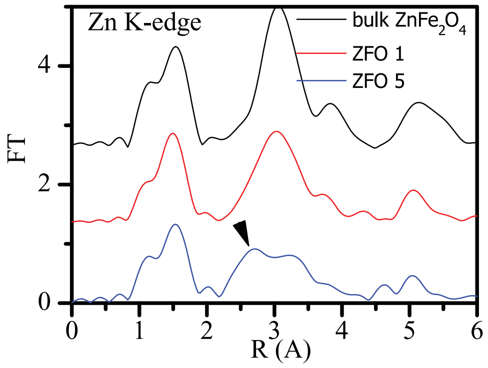

FIG. 6. (Color online) Fourier transforms of $k^2\chi(k)$ oscillations (Zn K edge) of bulk $ZnFe_2O_4$, ZFO1, and ZFO5 film ferrites. The arrow indicates the new coordination appearing in the FT of sample ZFO5, which indicates that there are Zn atoms at B sites.

Regarding XANES results, we can conclude that in the films grown at low pressure, Zn^{2+} ions are in A sites (coordination 4) and Fe^{3+} are octahedrally (B site) and tetrahedrally coordinated (A site). Also, there is a fraction of Fe^{2+} probably in B sites such as in Fe_3O_4 structure. The increase of Fe^{3+} in A sites and Fe^{2+} is favored by the deposition at low oxygen pressure and then due probably to the oxygen-vacancy formation. A probe of that is the decrease of features in the XANES Fe K edge taken with incidence angles lower than the total reflection one, i.e., corresponding to the surface region where available environmental oxygen neutralizes oxygen vacancies. Then, in the case of low-pressure growth films, there is an increase of Fe^{3+} tetrahedral sites without inversion.

This significant result is supported by EXAFS. Figure 6 shows the Fourier transform (FT) of oscillations extracted from a Zn k edge using the Athena program of ZFO1 and ZFO5 films compared with FT of bulk $ZnFe_2O_4$.

FT of sample ZFO1 is qualitatively equal to bulk $ZnFe_2O_4$, reasserting that Zn atoms are in the tetrahedral sites. In the case of ZFO5, the presence of an additional peak around 2.6 A is an indication that there are Zn atoms at octahedral sites.[5]

The situation is different from the scenario found in Refs. 5 and 9: when Zn occupancy of 8-sites increases, Fe decreases, indicating some degree of inversion and magnetic response enhanced with such inversion. In our case, the increase of Fe^{3+} in A sites is not due to Zn and Fe ion inversion, but the mechanism that explains the increase in the magnetization is probably the same as the one reported for the inverse spinel. The increase of Fe^{3+} tetrahedrally coordinated (A site) increases Fe^A-Fe^B pairs antiferromagnetically coupled by superexchange, forcing Fe^B-Fe^B pairs to align ferromagnetically and also because Fe individual magnetic moments probably no longer cancel. The experimental results reported in this work suggest that the increase of Fe^{3+} in A sites is not due to Zn and Fe ion inversion but to iron situated on normally nonoccupied A sites in the spinel structure. In this structure, only one-eighth of the A sites in a unit cell are actually occupied, and so some iron ions at these normally unoccupied sites will act as impurities and will not influence the crystallographic properties.

One more aspect in which oxygen pressure could have an influence is that as the magnetic interaction in the spinel is an indirect interaction, missing oxygen gives rise to a variation of exchange fields for the ions and a spin-glass-like state is formed. Also, the reduction of Fe^{3+} ions into Fe^{2+} ions located in octahedral sites would strengthen ferromagnetic coupling between B-B sites; such is the case in magnetite. In the case of Fe^{2+} located on the *A* sites, there is an increase of magnetic moment due to the antiferromagnetic coupling with Fe^{3+}, but the change will not be as big as for antisites.

In summary, we have shown that ferrites grown under low O_2 pressure conditions have a large magnetic moment. We found that the inversion mechanism is not responsible for the enhancements of the magnetic interaction—as was found in similar systems—but the presence of defects as oxygen vacancies or iron situated on normally nonoccupied *A* sites in the spinel structure. We have also shown that by controlling the oxygen pressure during the deposition, it is possible to obtain conductive or insulating Zn ferrites. These findings allow us to control the magnetic and electric transport properties of spinel ferrites controlling the oxygen concentration.

ACKNOWLEDGMENTS

We thank Silvana Stewart for fruitful discussions and Azucena Mudarra Navarro for collaboration in the XAFS experiments. This work was partially supported by Laboratorio Nacional de Luz Sincrotron, Campinas-Brasil, by CIUNT under Grant No. 26/E439, by ANPCyT-PICTR 20770 and 35682, by the German-Argentine PROALAR Grant No. D/08/11707, and the Collaborative Research Center SFB 762 "Functionality of Oxide Interfaces."

---

[*] Also at On leave from I.N.T.I.-CONICET, Av. Gral. Paz 5445 Ed. 42, B1650JKA, San Martín, Bs As.

[1] A. Yanase and K. Siratori, J. Phys. Soc. Jpn. **53**, 312 (1984).

[2] U. Lüders, A. Barthélémy, M. Bibes, K. Bouzehouane, S. Fusil, E. Jacquet, J. P. Contour, J.-F. Bobo, J. Fontcuberta, and A. Fert, Adv. Mater. **18**, 1733 (2006).

[3] S. Ayyappan, S. Philip Raja, C. Venkateswaran, J. Philip, and B. Raj, Appl. Phys. Lett. **96**, 143106 (2010).

[4] C. Yao, Q. Zeng, G. F. Goya, T. Torres, J. Liu, H. Wu, M. Ge, Y. Zeng, Y. Wang, and J. Z. Jiang, J. Phys. Chem. C **111**, 12274 (2007).

[5] S. J. Stewart, S. J. A. Figueroa, J. M. Ramallo López, S. G. Marchetti, J. F. Bengoa, R. J. Prado, and F. G. Requejo, Phys. Rev. B **75**, 073408 (2007).

[6] J. H. Shim, S. Lee, J. H. Park, S. J. Han, Y. H. Jeong, and Y. W. Cho, Phys. Rev. B **73**, 064404 (2006).

[7] V. Blanco-Gutiérrez, F. Jiménez-Villacorta, P. Bonvilles, R. Torralvo-Fernández, and M. J. Saez-Puche, J. Phys. Chem. C **115**, 1627 (2011).

[8] T. Kamiyama, K. Haneda, T. Sato, S. Ikeda, and H. Asano, Solid State Commun. **81**, 563 (1992).

[9] S. Nakashima, K. Fujita, K. Tanaka, K. Hirao, T. Yamamoto, and I. Tanaka, Phys. Rev. B **75**, 174443 (2007).

[10] Y. F. Chen, D. Spoddig, and M. Ziese, J. Phys. D **41**, 205004 (2008).

[11] F. K. Lotgering, J. Phys. Chem. Solids **27**, 139 (1966).

[12] S. Ligenza, Phys. Status Solidi **75**, 315 (1976).

[13] A. Kundu, C. Upadhyay, and H. Verma, Phys. Lett. A **311**, 410 (2003).

[14] S. D. Shenoya, P. A. Joyb, and M. R. Anantharaman, J. Magn. Magn. Mater. **269**, 217 (2004).

[15] J. Takaobushi *et al.*, Appl. Phys. Lett. **89**, 242507 (2006).

[16] K. Kamazawa, Y. Tsunoda, H. Kadowaki, and K. Kohn, Phys. Rev. B **68**, 024412 (2003).

[17] V. Fernandes *et al.*, Phys. Rev. B **80**, 035202 (2009).

[18] M. Khalid *et al.*, Phys. Rev. B **80**, 035331 (2009).

[19] M. A. Ramos, J. Barzola Quiquia, P. Esquinazi, A. Muñoz-Martin, A. Climent-Font, and M. García-Hernández, Phys. Rev. B **81**, 214404 (2010).

[20] H. Ohldag, P. Esquinazi, E. Arenholz, D. Spemann, M. Rothermel, A. Setzer, and T. Butz, New J. Phys. **12**, 123012 (2010), and references therein.

[21] M. Sultan and R. Singh, J. Appl. Phys. **105**, 07A512 (2009).

[22] D. Darko Makovec, A. Alojz Kodre, I. Iztok Arcon, and M. Miha Drofenik Darko, J. Nanopart. Res. **13**, 1781 (2011).

[23] S. J. A. Figueroa and S. J. Stewart, J. Synchrotron Radiat. **16**, 63 (2009).

[24] M. Akhatar, M. Nadeem, S. Javaid, and M. Atif, J. Phys. Condens. Matter **21**, 405303 (2009).

[25] J. Als-Nielsen, D. Jacquemain, K. Kjaer, F. Leveiller, M. Lahav, and L. Leiserowitz, Phys. Rep. **246**, 251 (1994).

[26] K. Stoev and K. Sakurai, Spect. Acta Part B **54**, 41 (1999).

[27] N. Souza-Neto, A. Y. Ramos, H. Tolentino, and Y. Joly, J. Phys.: Conf. Series. **190**, 012112 (2009).

[28] B. Henke, E. Gullikson, and J. Davis, At. Data Nucl. Data Tables **54**, 181(1993).